THE PENNSYLVANIA STATE UNIVERSITY
SCHREYER HONORS COLLEGE

DEPARTMENT OF ENGINEERING SCIENCE AND MECHANICS

FERROELECTRIC FIELD EFFECT TRANSISTORS: NEGATIVE CAPACITANCE FOR EFFICIENT SWITCHING

VICTORIA LI CHIEN CHEN
SPRING 2016

A thesis
submitted in partial fulfillment
of the requirements
for a baccalaureate degree
in Engineering Science
with honors in Engineering Science

Reviewed and approved* by the following:

Suman Datta
Professor of Electrical Engineering
Thesis Supervisor

Gary Gray
Professor of Engineering Science
Honors Adviser

* Signatures are on file in the Schreyer Honors College.

ABSTRACT

In recent years, there has been an increasing number of issues associated with the continued Metal Oxide Semiconductor Field Effect Transistor (MOSFET) scaling. As feature lengths shrink down to atomic sizes, problems with power consumption, heat dissipation, and quantum effects become more prevalent. The unique properties of ferroelectric materials and their ability to display a negative differential capacitance make them a promising candidate for the use in future transistor technology, and a potential successor to traditional silicon CMOS devices. By placing a ferroelectric material layer in place of the dielectric layer of a MOSFET, it is possible to achieve a subthreshold slope lower than the typical 60 mV/dec limit. This device is called a ferroelectric field effect transistor (FerroFET). In this work, we develop a computational model based on the Landau-Devonshire theory to extract Landau coefficients from polarization-voltage data of a ferroelectric capacitor and simulate the current-voltage behavior of a FerroFET. We computationally demonstrate the gains of FerroFETs over conventional CMOS devices and explore properties of various ferroelectric materials. These FerroFETs have great potential for use in low power applications and could greatly revolutionize the current semiconductor industry.

TABLE OF CONTENTS

LIST OF FIGURES

LIST OF TABLES

ACKNOWLEDGEMENTS

I would like to thank my research advisor Professor Suman Datta for giving me the opportunity to conduct research in his group. The experience with these nanoelectronic devices has been invaluable and has led to many more opportunities in the field, contributing to my decision to go to graduate school for Electrical Engineering. I would also like to thank my post-doctoral mentors Sandeepan Dasgupta and Swapnadip Ghosh for all of their patient explanations of the concepts and for sharing their data.

Chapter 1: Literature Review

1. Background and Limitations of Current MOSFET Technologies

The Metal Oxide Semiconductor Field Effect Transistor (MOSFET) has been an integral part of technological advancement in recent decades. The device uses an applied voltage to the gate terminal to modulate the drain current, and has been so remarkably successful in part due to its scalability [1]. By doping the semiconductor with different elements, NMOS and PMOS devices can be fabricated so that the drain current can be composed of either electrons or holes as charge carriers, and circuits with both types of devices are called Complementary MOSFETs (CMOS). The structure of the MOSFET has remained relatively constant since its creation, and previous limitations with CMOS technologies have been overcome through materials engineering. For example, leakage current caused by quantum tunneling, which occurred for gate dielectric thicknesses at approximately 1 nm, could be countered by using materials with a higher dielectric constant [1]. This allows for a greater oxide capacitance without having to further decrease the thickness of the oxide layer.

However, in recent years the scaling has slowed as the limits to conventional CMOS technology are reached. Microprocessor clock frequencies had increased exponentially for nearly 20 years, but in 2005 reached a plateau when the rate of improvement greatly decreased [2]. Power dissipation is also a major issue, with both active and passive power contributing to the power per chip that must be removed [1]. In addition, as devices continue to be made smaller, the threshold voltage V_{th} must also be reduced so that the ON/OFF current ratio is acceptable.

However, decreasing V_{th} has the undesirable result of exponentially increasing the OFF current and creating leakage issues [2]. To combat some leakage currents that result from electron tunneling through the gate when the insulator layer is made very thin, dielectric materials with a high permittivity were brought into use. This solution has allowed for some continued scaling, but will also not allow for indefinite feature size reductions [2].

The major objective is now to design a device that can overcome these limitations of conventional MOSFET technology. Ideally, the device will have a lower subthreshold slope than the 60 mV/dec boundary experienced by standard FETs, meaning that it will require less than 60 mV at 300 K to change the drain current by a factor of 10. Boltzmann statistics have fundamentally imposed restrictions on MOSFET operation with this limited subthreshold slope, and it is necessary to develop the next generation of devices that can operate beyond the present boundaries. Ferroelectric Field Effect Transistors (FerroFETs) have properties that make them an appealing candidate to serve as a successor to the MOSFET [3]. These novel devices incorporate a ferroelectric material layer as the gate insulator, which leads to a possible subthreshold slope lower than 60 mV/dec [2].

2. Ferroelectric Capacitors

When a voltage is applied to two metal terminals separated by a dielectric material, the positive and negative charges within the dielectric separate and the material polarizes. This is the concept behind a simple dielectric capacitor. Ferroelectric materials have a nonlinear polarization, so that small changes in the applied voltage can result in relatively large changes in the ferroelectric polarization [4]. This occurs due to the phase transition of the ferroelectric

between polar and nonpolar states, where the polarizability greatly increases. The spontaneous polarization that reverses above a specific critical voltage (coercive voltage) results in an accumulation of bound charge at the surface of the material, which can continue to increase while the applied voltage decreases [4]. There is an energy barrier that occurs due to the gate stack to charge injection, which is dependent on how the ferroelectric material is polarized [2]. Since capacitance is calculated by dividing the voltage by the charge between two layers, the result is a negative differential capacitance across the ferroelectric. This phenomenon is illustrated in Figure 1, with a ferroelectric capacitor on the left undergoing polarization states plotted to the right.

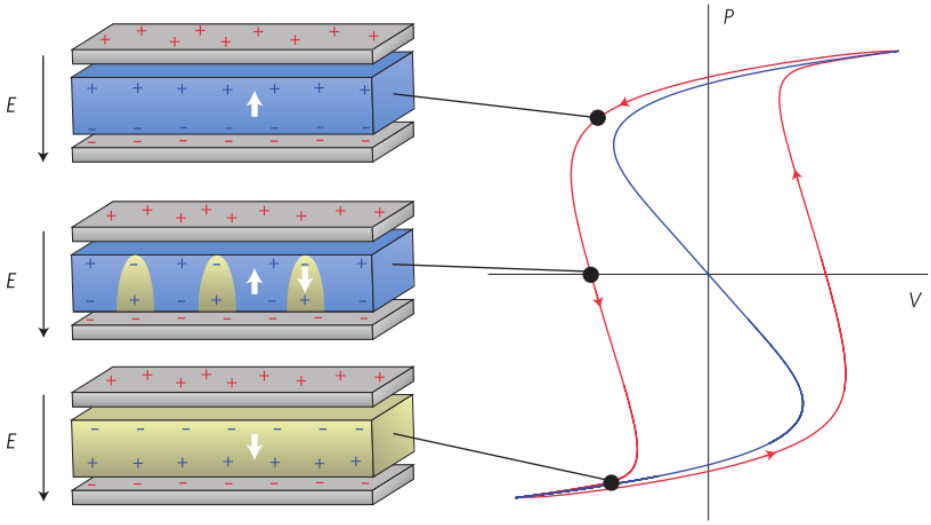

Figure 1 A ferroelectric capacitor is shown on the left, with the white arrows signifying the direction of polarization. The growth of domains results in the ferroelectric undergoing a reversal of its polarization direction. The plot on the right shows the polarization as a function of the internal ferroelectric node voltage (blue) and the voltage across the ferroelectric capacitor (red), as well as points corresponding to the charge distributions shown on the left. Figure reproduced from ref. 4, 2015 Nature Materials.

This negative differential capacitance generally occurs in materials with very high dielectric constants, and while the negative capacitance state of the ferroelectric capacitor is

unstable, it can be stabilized with the use of a dielectric capacitor in series [5]. A group at UC Berkeley led by Professor Sayeef Salahuddin placed a ferroelectric capacitor in series with a resistor, applied a voltage pulse, and measured the change in the resulting polarization [5]. The ferroelectric material $Pb(Zr_{0.2}Ti_{0.8})O_3$ (PZT) was 60 nm thick and grown on another 60 nm thick $SrRuO_3$ – buffered $SrTiO_3$ substrate, and the resistor used in series was 50 kΩ [5]. Due to parasitic effects of the probe station and oscilloscope, there is an additional capacitance contributed in parallel to the ferroelectric capacitor. Then, the sum of the charge in the ferroelectric and parasitic capacitors is a function of time and is given by the expression: $Q(t) = \int_0^t i_R(t)dt$ where $i_R(t)$ is the current that flows through the 50 kΩ resistor [5]. By measuring the voltage across the ferroelectric capacitor, V_F, the charge across the ferroelectric can then be calculated as $Q_F(t) = Q(t) - CV_F(t)$.

When a voltage pulse from -5.4 V to +5.4 V to -5.4 V was applied, there was a brief window where the voltage across the ferroelectric capacitor V_F and the charge within it Q were changing in opposite directions [5]. This leads to a negative dQ/dV_F value, and therefore negative differential capacitance. These results are shown in Figure 2, where the polarization is plotted against the voltage across the ferroelectric, and calculated as the charge density, determined by the expression $P(t) = Q_F(t)/A$.

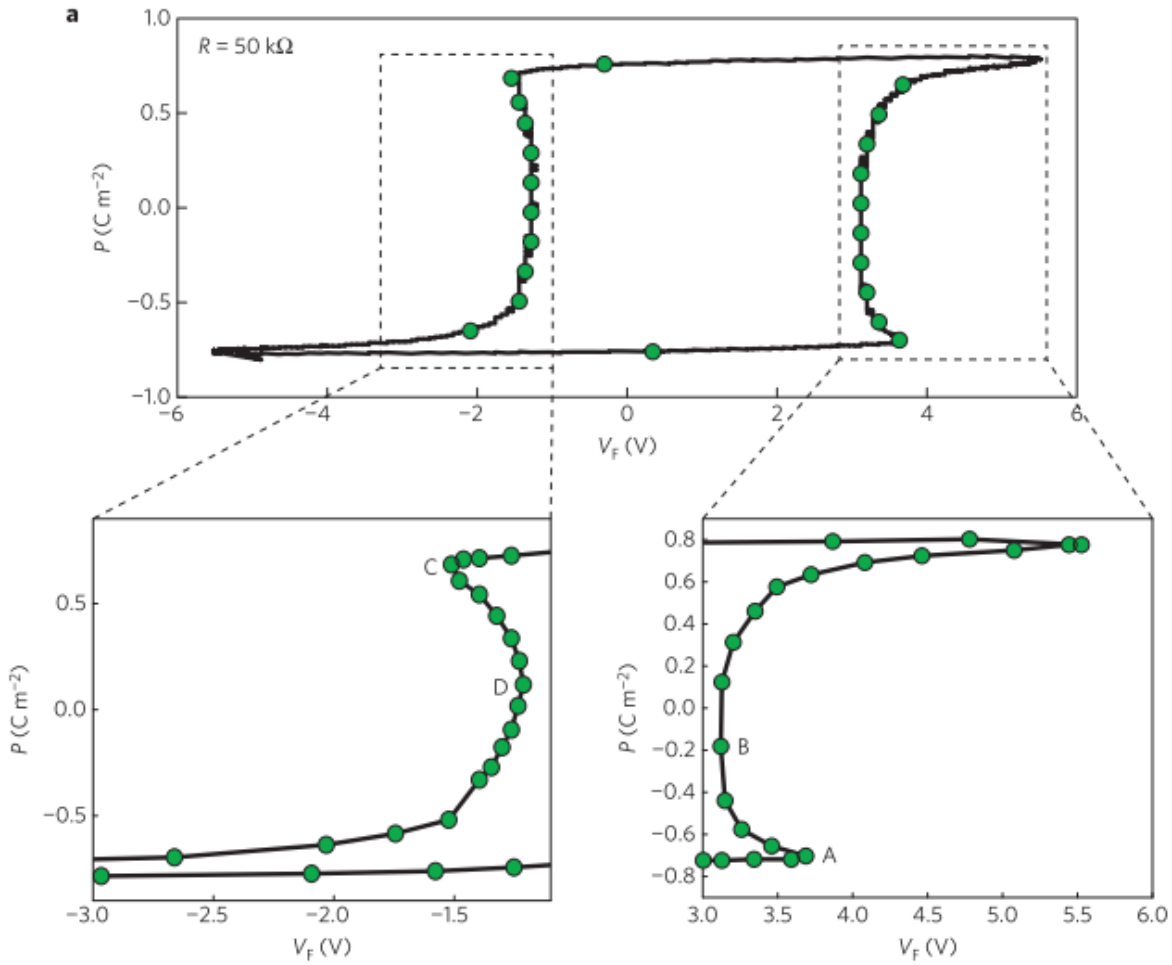

Figure 2 Experimental results of polarization P(t) plotted against $V_F(t)$ with an applied voltage pulse. In the regions marked AB and CD, the value of dP/dV_F is negative, and therefore there is a negative differential capacitance between those points. Figure reproduced from ref. 5, 2014 Nature Materials.

This unique property of ferroelectric capacitors has the potential to solve some of the issues faced by current MOSFET technology. Not only would a lower switching voltage conserve energy, but also since heat dissipation is a major concern with the smaller and faster transistors, a solution would be to lower the required voltage applied to the gate [4]. Using negative capacitance from the ferroelectric, the lower gate voltage could be effectively amplified to allow for a lower voltage device operation.

3. Landau Theory

Landau theory was developed in the 1930s as a model to describe the equilibrium behavior of a system near a phase transition using an analysis based on symmetry [6]. It effectively provides a link between the microscopic models and what is observed macroscopically. This theory is particularly appropriate for homogenous and bulk ferroelectric materials because it relies on a special averaging of the local fluctuations [6]. To characterize the paraelectric-ferroelectric phase transition, Landau theory expands the free energy expression as a power series with respect to the order parameter P, which is the polarization [6].

The first application of Landau theory specifically to ferroelectrics was done by Devonshire, leading to the Landau-Devonshire theory for bulk, single crystal ferroelectrics with uniform polarization [6]. Neglecting the strain field, which is accurate for a uniaxial ferroelectric material, and excluding higher order terms after the sixth, the free energy can be written as

$$F_P = \frac{1}{2}aP^2 + \frac{1}{4}bP^4 + \frac{1}{6}cP^6 - EP$$

where a, b, and c are constant coefficients. This expression is a relatively accurate and concise statement of the free energy, where the energy origin for a free, unpolarized, and unstrained crystal is zero [6]. A comparison of the free energy plotted against polarization is shown in Figure 3 for two different material types.

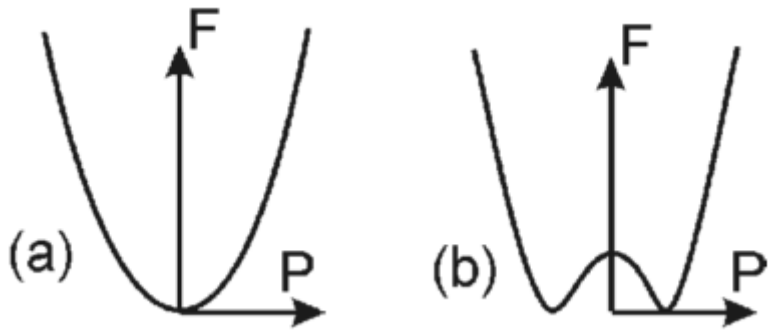

Figure 3 Plots of free energy versus polarization for (a) a paraelectric material and (b) a ferroelectric material. Figure reproduced from ref. 6, 2008 A Landau Primer for Ferroelectrics.

The equilibrium point of the free energy occurs at the minima of the function, and this can be determined by

$$\frac{\partial F_P}{\partial P} = 0$$

which yields a function that gives the electric field E as a function of the polarization P

$$E = aP + bP^3 + cP^5$$

From the above expression, with measured polarization data of a ferroelectric material under an applied electric field, the constants a, b, and c (which are also referred to as α, β, and γ) can be experimentally determined. These values are then used to extrapolate and simulate the behavior of a ferroelectric material in different contexts.

In addition, the size of the ferroelectric material can influence its dielectric constant [7]. For example, in lead titanate, the maximum dielectric constant occurs when the material has an average grain size of 100 nm [7]. Material thickness can have an effect on susceptibility, spontaneous polarization, and Curie temperature, so this must also be kept in mind while generating models for ferroelectric material behavior [7].

4. Ferroelectric Field Effect Transistors

The Ferroelectric Field Effect Transistor (FerroFET) is a device that is similar in structure to the MOSFET but replaces the dielectric layer with a ferroelectric material. In some instances, a high-κ dielectric is also inserted as a buffer interlayer between the ferroelectric and semiconductor [8]. Because of the differential negative capacitance possible across the ferroelectric layer, it becomes possible to obtain a subthreshold slope in a FerroFET less than the 60 mV/dec conventional MOSFET limit. The negative capacitance across the ferroelectric material layer is in series with the positive capacitance across the semiconductor, summing to allow the device current to increase at much higher rates than previously possible in standard MOSFETs [8].

Recently, a FerroFET using $PbZr_{0.52}Ti_{0.48}O_3$ (PZT) as the ferroelectric gate insulator and HfO_2 as a buffer layer showed incredibly steep slope switching, attaining 13 mV/dec at 300K in strong inversion [8]. This behavior is consistent with the predictions from Landau-Devonshire theory, confirming the feasibility of FerroFET devices despite approximations in the model and the fact that the Landau-Devonshire theory describes single crystal ferroelectrics, rather than polycrystalline ones such as PZT.

This FerroFET was fabricated on (100) p-type silicon with Phosphoryl chloride ($POCl_3$) diffusion for doping the n-type source and drain. The HfO_2 layer was 10 nm thick and deposited between the ferroelectric and substrate layer in order to prevent any reactions between them, and the PZT layer was 100 nm thick [8]. Although it would be ideal for the PZT and HfO_2 layers to be thinner, the oxide needed to be thick enough such that the Pb could not diffuse through and react with the substrate during the rapid thermal annealing at a high temperature. In addition, the

ferroelectric layer had to be thick enough to have a significant negative capacitance contribution [8].

The steep switching, approximately 13 mV/dec, for the PZT FerroFET with a 10 µm channel length occurred in strong inversion when V_{gs} = 12.6 V [8]. A hysteresis of approximately 10 V was required for turn off [8]. These values, along with the I_d-V_g characteristics of the device, provide empirical evidence confirming the relative accuracy of models based on the Landau-Devonshire theory. Experimental data is shown in Figure 4.

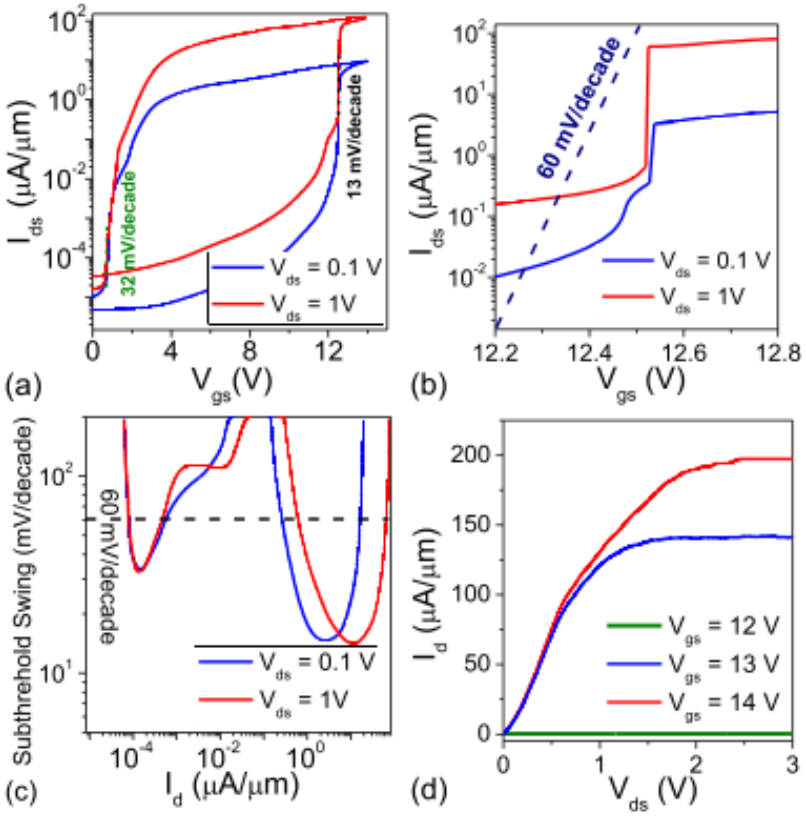

Figure 4 (a) I_d-V_g characteristics of a FerroFET with PZT as the gate insulator and 10 µm channel length for V_{ds} = 0.1 V and V_{ds} = 1 V. (b) Limited x-domain of the same plot showing the steep turn on and off. (c) Very low subthreshold swing observed during strong inversion. (d) I_d-V_d characteristics showing saturation. Figure reproduced from ref. 8, 2015 IEEE.

The device's precise mechanism of switching can be understood by first separately examining characteristics of the ferroelectric capacitor and baseline silicon MOSFET. The Q-V characteristics of the standard Si FET can be obtained by experimentally measuring the C-V characteristics and integrating [8]. Then, the accumulation capacitance is removed from the total capacitance so that the Q-V relationship for the baseline Si FET is determined with the effect of the oxide capacitance [8]. Q-V data is also obtained for the ferroelectric capacitor, and the ferroelectric and Si FET are combined in series to produce an approximation for the behavior of the corresponding FerroFET [8]. The FerroFET model is further explored computationally in this work with experimental data from various ferroelectric capacitor materials.

Chapter 2: Extracting Landau Coefficients of Ferroelectric Capacitors

1. Experimental Data from Ferroelectric Capacitors

As discussed previously, the first goal of this work is to determine the Landau coefficients α, β, and γ from the Landau Khalatnikov (LK) equation, given below:

$$E = \alpha P + \beta P^3 + \gamma P^5$$

The polarization versus electric field values in the LK equation are experimentally measured from different ferroelectric capacitor materials. The polarization and electric field data presented in this work were measured with a Radiant system. A triangular wave is input with the applied voltage range sweeping from -10 V to 10 V, and the corresponding charge can then be determined. While there are numerous methods to measure the P-E hysteresis loop of a ferroelectric, one relatively simple method uses a Sawyer-Tower circuit to integrate the current so that the measured voltage is proportional to the charge [9]. A Sawyer-Tower circuit is shown in Figure 5, where the ferroelectric capacitor and linear capacitor (sense capacitor) are in series with each other and located between the stimulus signal and ground [10]. The sense capacitor is chosen to reduce noise from the signal but remain small compared to the stimulus voltage so that the voltage across the ferroelectric capacitor can still be accurately measured [10]. Typically, capacitance values on the order of 5 nF are appropriate [10].

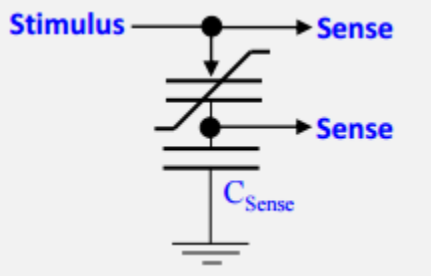

Figure 5 Sawyer-Tower Circuit. The upper capacitor is the ferroelectric, and the lower sense capacitor is linear. Figure reproduced from ref. 10, 2016 Radiant Technologies, Inc.

The structure pictured in Figure 6(a) is a ferroelectric capacitor with a 100 nm thick lead zirconium titanate (PZT) layer deposited onto a 10 nm thick dielectric HfO_2 layer. The top electrode is nickel and the bottom electrode is heavily doped Si++. Sputter deposition with an argon pressure of 2.5 mT was used to deposit the PZT onto the HfO_2. The crystallization temperature was 620°C and the voltage sweeps were done with a triangular pulse that had a 1 ms period. Placing a dielectric layer between the ferroelectric material and semiconductor serves to prevent the lead in the PZT from diffusing into the substrate material and reacting at high temperatures.

The hysteretic polarization versus voltage loops for this structure are shown in Figure 6(b) with -2 V to 2 V sweeps to -22 V to 22 V sweeps. The larger voltage sweeps tend have more symmetrical hysteresis loops with rounded corners, and in general have more accurate LK fits.

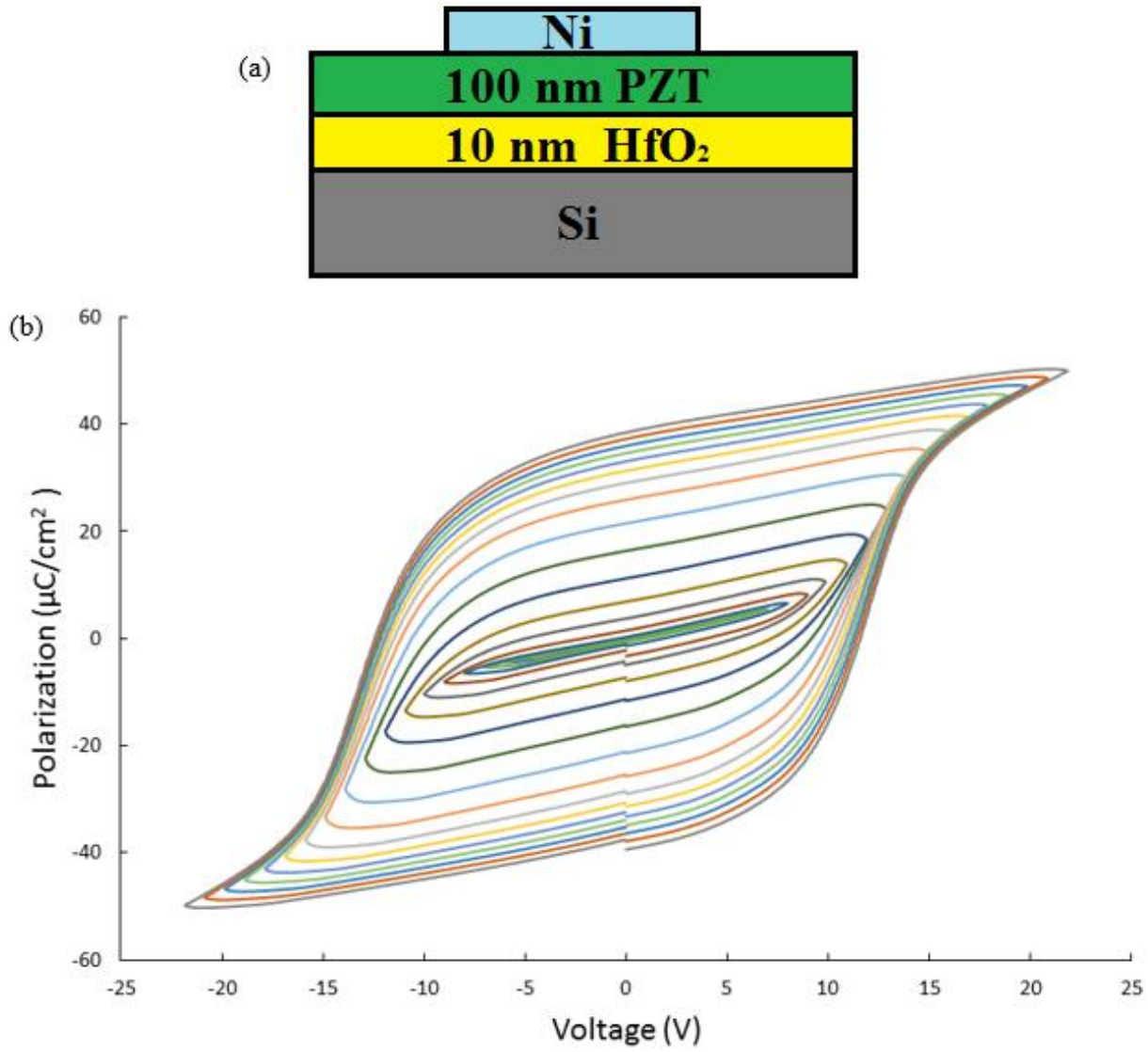

Figure 6 (a) A ferroelectric capacitor composed of a 100 nm layer PZT deposited on 10 nm HfO_2. (b) The experimentally measured polarization versus voltage hysteresis loops from the structure described in (a).

Decreasing the thickness of the PZT layer deposited on HfO_2 yields differently shaped hysteresis loops when polarization is measured against applied voltage sweeps. Figure 7 shows the polarization versus voltage curves for the same Ni/PZT/10 nm HfO_2/Si++ structure, but with varying thicknesses of PZT. The sputter deposition process for 50 nm and 35 nm PZT both had argon pressures of 2.5 mT. The crystallization temperature for 50 nm PZT was 620°C, and the

crystallization temperature for 35 nm PZT was 590°C. Both structures were characterized with triangular voltage pulses that had a 1 ms period.

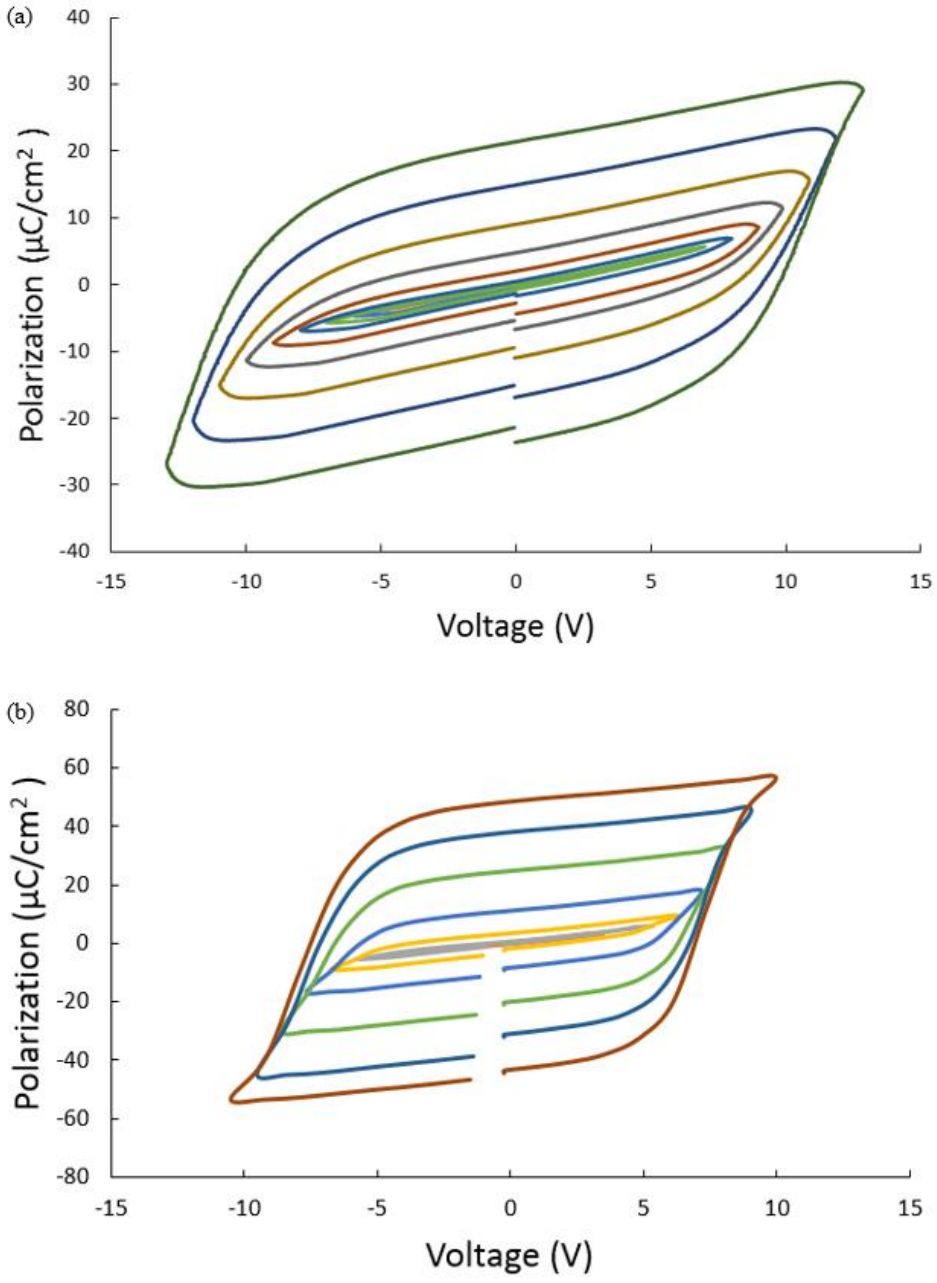

Figure 7 Polarization versus voltage curves for the capacitor structure with (a) 50 nm of PZT deposited on 10 nm of HfO_2 and (b) 35 nm of PZT deposited on 10 nm of HfO_2

Adding a layer of the transition metal platinum between the ferroelectric and dielectric layers changes the physical structure of the material and therefore has an impact on the electrical characteristics. When PZT is deposited on Pt, the average grain dimension becomes approximately three times smaller than that of PZT deposited directly on HfO_2. This is because Pt has a lower nucleation barrier for PZT than HfO_2, and reducing the grain size allows the PZT to switch at lower voltages. Scanning Electron Microscope images of the two structure types are shown in Figure 8 and illustrate the differences in grain sizes.

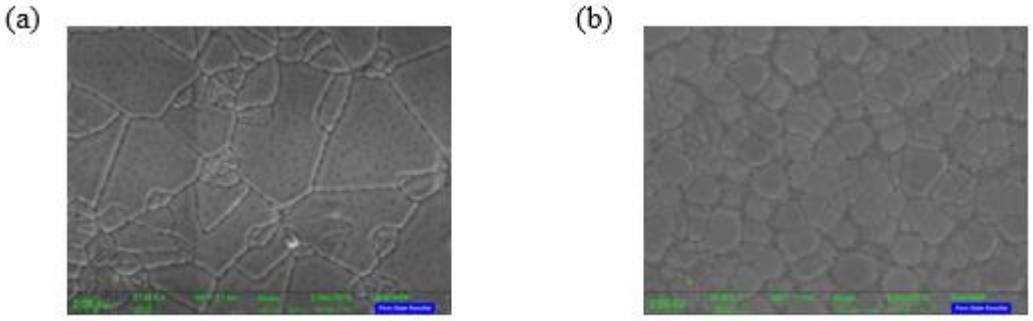

Figure 8 SEM images for a structural comparison of PZT deposited on (a) HfO_2 and (b) Pt

The coercive voltage is seven times smaller in the Ni/PZT/Pt/HfO_2/Si++ ferroelectric capacitor than in the Ni/PZT/HfO_2/Si++ ferroelectric capacitor. The polarization versus voltage curves for this type of structure are much narrower and are plotted in Figure 9 for PZT thicknesses of 100 nm and 50 nm.

These hysteresis loops for the PZT deposited on Pt ferroelectric capacitors are shifted laterally and not centered at the origin because of the work function difference between the heavily doped silicon electrode (~4.05eV) and the nickel electrode (~5.04 eV). For the later LK fit calculations, the curves are appropriately shifted to be centered at the origin. The ferroelectric capacitor structures are also pictured in Figure 9.

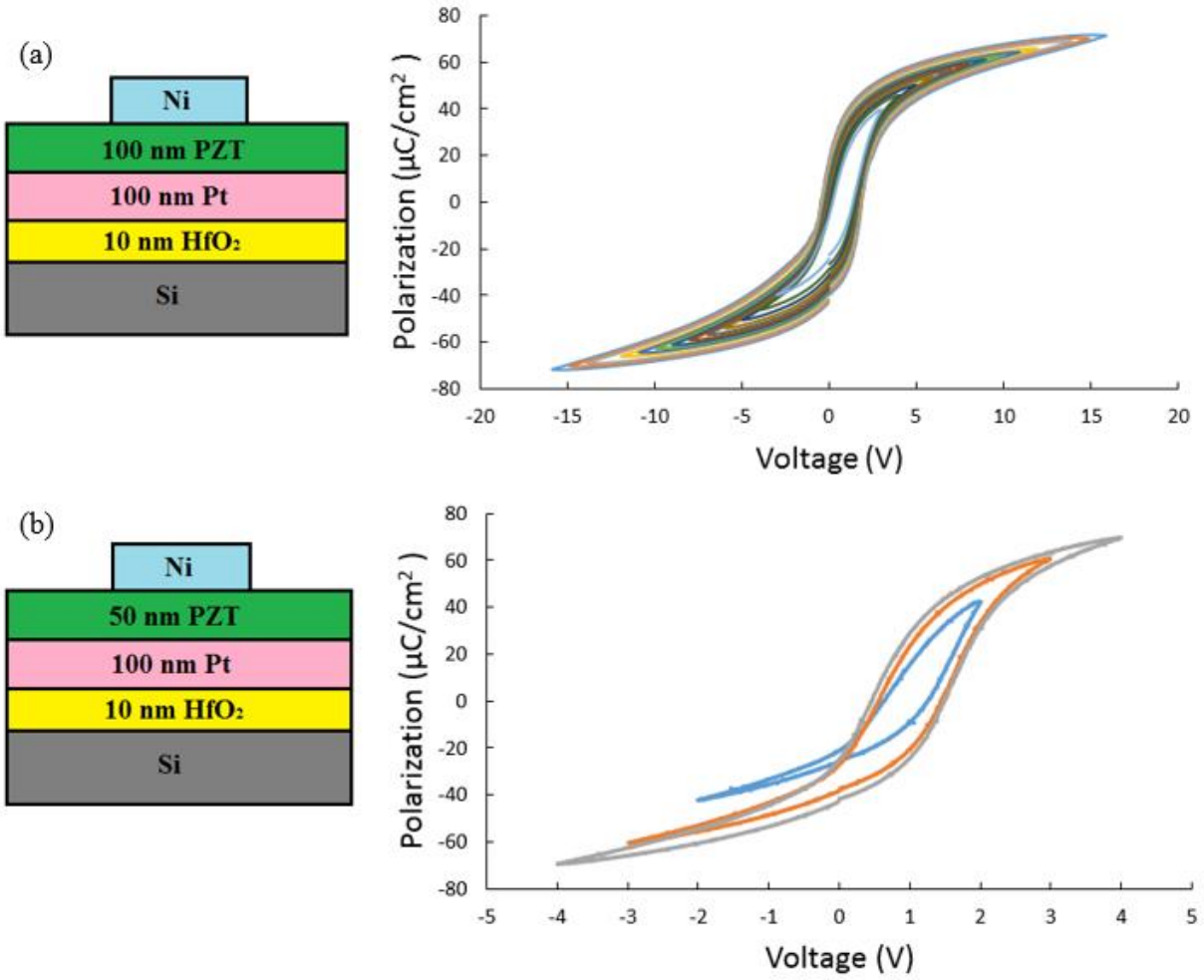

Figure 9 Ferroelectric capacitor structures on the left and their corresponding polarization versus voltage hysteresis loops on the left. (a) 100 nm of PZT deposited on 100 nm Pt. (b) 50 nm PZT deposited on 100 nm Pt.

Varying the thickness of the Pt layer also affects the electrical characteristics of the ferroelectric capacitor, and Figure 10 shows the polarization versus voltage curves for 100 nm of PZT deposited onto 100 nm, 60 nm, and 35 nm Pt. The hysteresis loop that occurs even for thinner layers of Pt show an opportunity to potentially continue decreasing the thickness of the PZT layer in this ferroelectric capacitor, allowing for further scaling. The plots in Figure 10 were

experimentally measured from structures with titanium as one electrode (instead of nickel), with 100 nm of PZT deposited on varying thicknesses of Pt and 10 nm of HfO_2. As with the previous plots, these measurements were performed with a triangular wave with 1 ms period.

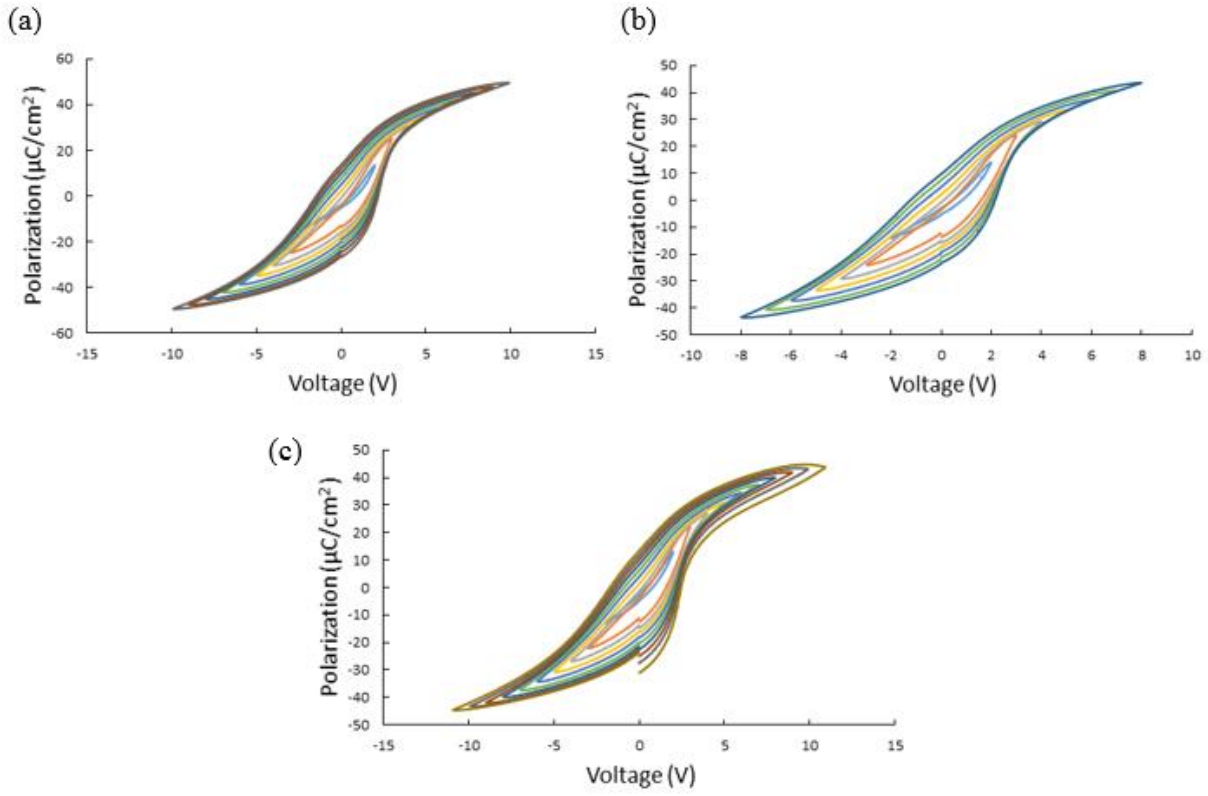

Figure 10 Polarization versus voltage curves for ferroelectric capacitors with 100 nm of PZT deposited on (a) 100 nm Pt, (b) 60 nm Pt, (c) 35 nm Pt.

2. Extracting Landau Coefficients: P-E Data Input Only

Using the polarization versus electric field data obtained in the previous section, a Matlab script was written to fit the LK curve to the data and extract the Landau coefficients of the ferroelectric capacitor. The script first determines which experimental data points to use in fitting

the LK curve, since the "unstable" region through the middle of the hysteresis curve contains values on the LK curve but not from the experimental data. The inflection points on the lower right and upper left of the P-E hysteresis curve correspond with the inflection points of the LK equation, and so identifying these points is key in obtaining an accurate fit. To do so, the script determines the minimum and maximum voltage values (the edges of the voltage sweep) and their corresponding polarization values. It then fits a linear line through the two points that divides the data into an upper and lower half. Because the data is now divided into two halves, each of the two data sets is a function and a tenth degree polynomial is then fit to the upper half data as well as the lower half data. This process shown in Figure 11, with a linear line dividing the measured data into two halves, each fit with a 10^{th} degree polynomial which is then used to determine the inflection points.

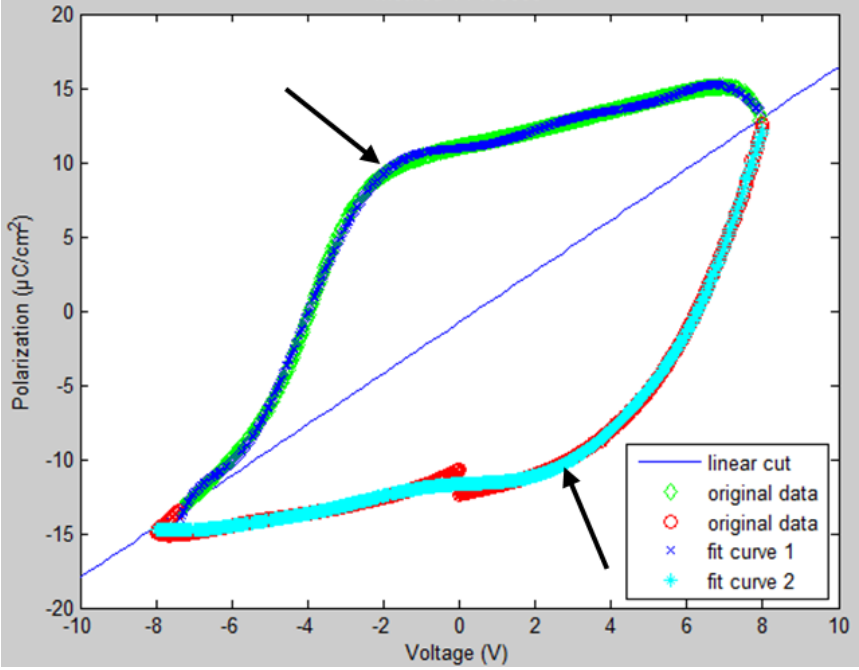

Figure 11 A polarization versus voltage hysteresis curve with a linear line dividing it into two halves. A 10^{th} degree polynomial is fit and superimposed onto each half, and these polynomials are used to find the inflection points, designated with arrows.

The points that will be used for the LK fit are the values from the minimum voltage to the lower inflection point, and upper inflection point to the maximum voltage. To find these inflection points, the first, second, and third derivative of each polynomial is calculated. The upper point occurs in the second quadrant when the first derivative is positive, the second is negative, and third is zero. The lower point occurs in the fourth quadrant when the first derivative is positive, the second is positive, and the third is zero. The data points to the correct side of the inflection point are then selected, as well as 10% of points from the opposite side for continuity purposes. The subset of polarization and voltage data points that are used for the LK fit are plotted in Figure 12.

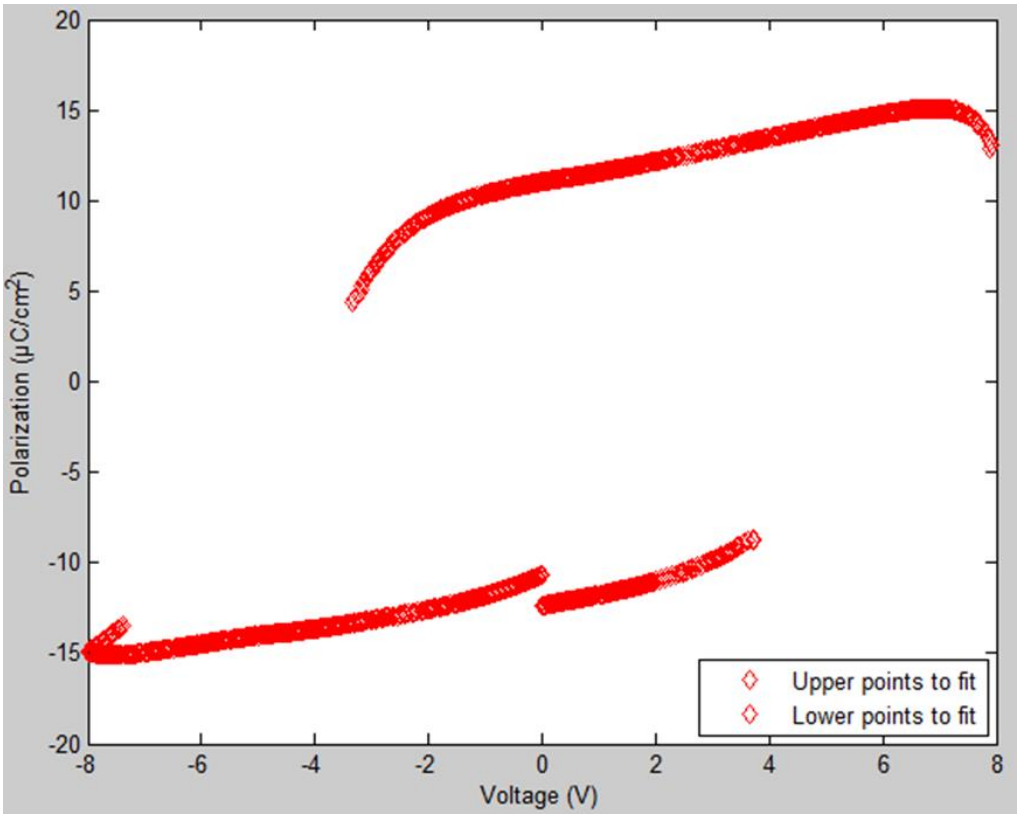

Figure 12 The subset of data points selected from the original data set that are used to compute the LK fit.

With this new set of points, the code uses a modified least squares regression method to determine the Landau coefficients α, β, and γ. This is done by setting the voltage matrix equal to the sum of the polarization matrix containing the first, third, and fifth powers of each polarization value multiplied by their respective Landau coefficients and the residuals. In the following matrix expression, n represents the number of data points, V is the applied voltage, P is the measured polarization, α, β, and γ are the Landau coefficients, and ε is the residual or error between the experimental data and ideal fit.

$$\begin{bmatrix} V_1 \\ V_2 \\ \dots \\ V_n \end{bmatrix} = \begin{bmatrix} P_1 & P_1^3 & P_1^5 \\ P_2 & P_2^3 & P_2^5 \\ \dots & \dots & \dots \\ P_n & P_n^3 & P_n^5 \end{bmatrix} \begin{bmatrix} \alpha \\ \beta \\ \gamma \end{bmatrix} + \begin{bmatrix} \varepsilon_1 \\ \varepsilon_2 \\ \dots \\ \varepsilon_3 \end{bmatrix}$$

To minimize the total residual, the partial derivatives of the sum of the residuals with respect to α, β, and γ are set equal to zero. These three equations are then solved to determine the three Landau coefficients. The equations are shown below:

$$S = \varepsilon_1^2 + \varepsilon_2^2 + \cdots + \varepsilon_3^2$$

$$\frac{\partial S}{\partial \alpha} = 0, \quad \frac{\partial S}{\partial \beta} = 0, \quad \frac{\partial S}{\partial \gamma} = 0$$

This method of calculating the Landau coefficients is effective for ideal polarization versus voltage loops. However, when there is asymmetry or corner rounding of the hysteresis loop (a non-ideal shape), the accuracy of the generated coefficients decreases. In this case, a

second script that requires additional user input can be used instead, and this is discussed in the next section.

3. Extracting Landau Coefficients: P-E Data and Additional User Input

This second Matlab script also accepts the ferroelectric capacitor P-E data as an input, but also requires additional user input in order to correct for non-ideal hysteresis loop shapes in which the inflection points are not apparent. The program plots the P-E data loop in a figure that gives the user a crosshair to select a minimum of six points (to define the fifth degree LK polynomial) that trace the desired LK curve. There is no maximum number of points that can be selected, so further points may be chosen to increase the accuracy of the fit. With these user defined points, the same modified least squares regression method as before is then implemented to solve for the Landau coefficients. Figure 13 shows the Matlab-generated user interface for selecting points of interest for the LK fit.

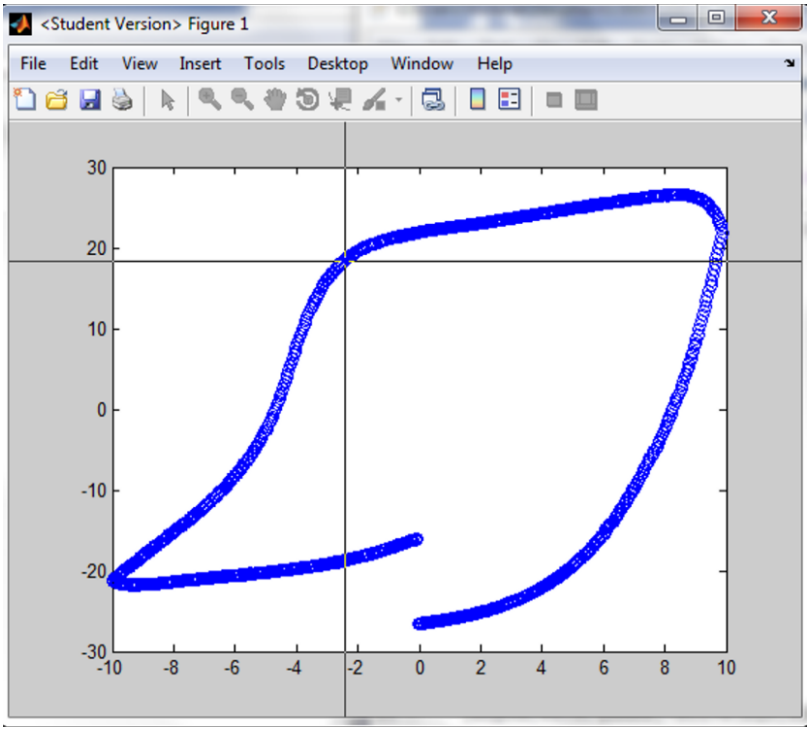

Figure 13 The user interface which plots the experimental P-V ferroelectric capacitor data and allows for the LK fit points to be specified.

This second method has the advantage of yielding relatively accurate Landau coefficient values for non-ideal polarization-voltage curves. In other words, when the hysteresis loop is narrow or the inflection points are not well defined, allowing the user to "trace" points on the desired LK fit curve can return more logical results. However, unlike the first method, because of the additional user input required, the second method may yield varying Landau coefficients on repeated runs on the same data if the user does not select the exact same points each time. The first method, where only the polarization versus voltage data is input, will output the same results for a specific data set with every run.

4. A Comparison of the Two Methods

The different levels of user input required for the two methods discussed previously can result in different LK fits and Landau coefficient values. Symmetric hysteresis loops with well defined inflection points generally result in similar LK fits regardless of the level of user input, and this is shown in Figure 14. Because the measured P-V loops were relatively symmetric, the LK fits by each of the methods yield very similar results.

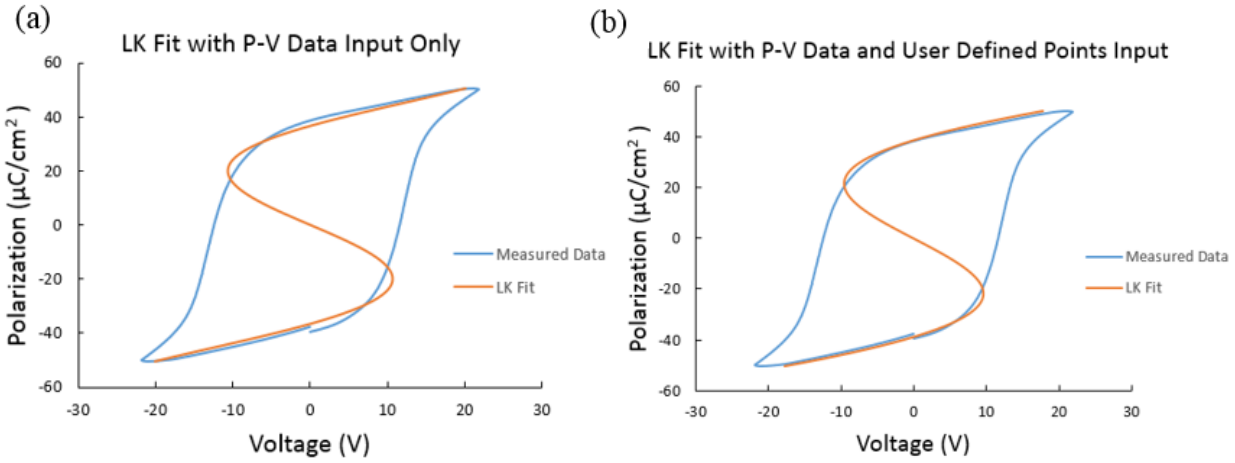

Figure 14 Measured polarization versus voltage data for 100 nm PZT deposited on 10 nm HfO_2 with computed LK fits superimposed. (a) LK fit computed with only P-V data input. (b) LK fit computed with P-V data and additional user defined points input.

Hysteresis loops that are not as symmetric or do not have very clearly defined inflection points will have more pronounced differences in the values of the calculated coefficients. An example of this is shown in Figure 15. Because the loop is extremely narrow, the code is unable to compute an accurate LK fit (with the negative capacitance region) when only the P-V data is

input. However, additional user input can help to define the inflection points and obtain a more accurate fit.

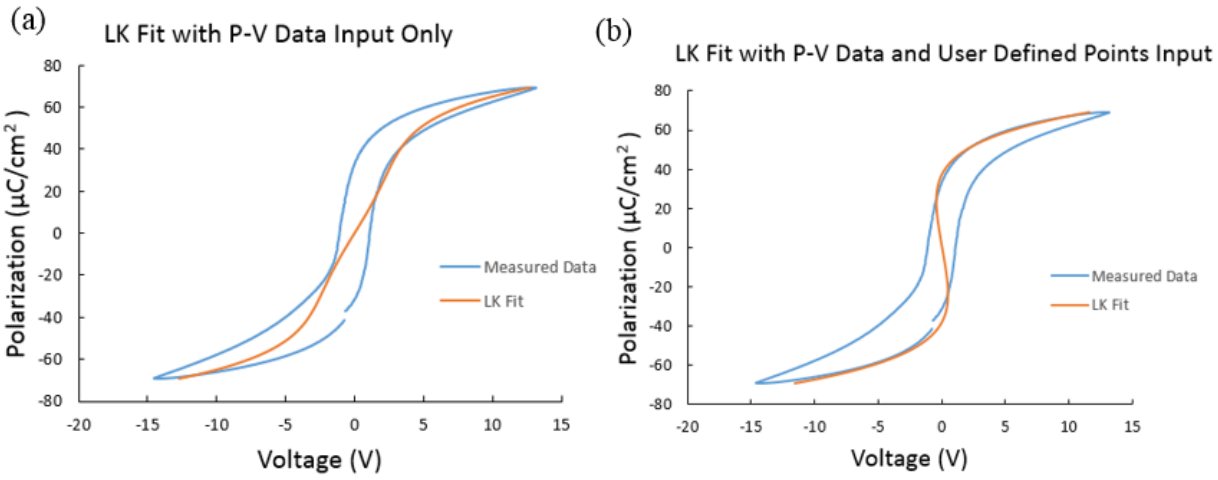

Figure 15 Measured polarization versus voltage data for 100 nm PZT deposited on 100 nm Pt with computed LK fits superimposed. (a) LK fit computed with only P-V data input. (b) LK fit computed with P-V data and additional user defined points input.

Chapter 3: LK Fits and Landau Coefficients from Experimental Data

1. PZT deposited on 10 nm HfO_2

Using the computational methods described in the previous section, this chapter presents the LK fits and Landau coefficients derived from experimental polarization versus voltage loops for various ferroelectric capacitors. Figure 16 shows plots that superimpose the calculated LK fit curves onto the measured polarization versus voltage hysteresis loops. These LK fit curves are based on the Landau coefficients α, β, and γ from the LK equation, and the polarization is plotted against voltage rather than electric field for consistency since voltage and electric field are proportional by the thickness of the ferroelectric. To obtain the most accurate fit, the largest voltage sweeps were used for each material type and thickness. This is because the inner loops of the polarization versus voltage plots were often too narrow to clearly see the hysteretic behavior because of the limited range of the voltage sweep. The computational methods described in the previous section yield the most accurate results with relatively symmetric loops that have clear inflection points. Since the measured data sets contain non-ideal hysteresis loop shapes, for consistency the method requiring additional user input to determine fit points was used to calculate all fits and coefficients. Figure 16 shows the LK fits for the 100 nm, 50 nm, and 35 nm thick PZT layers grown on 10 nm HfO_2.

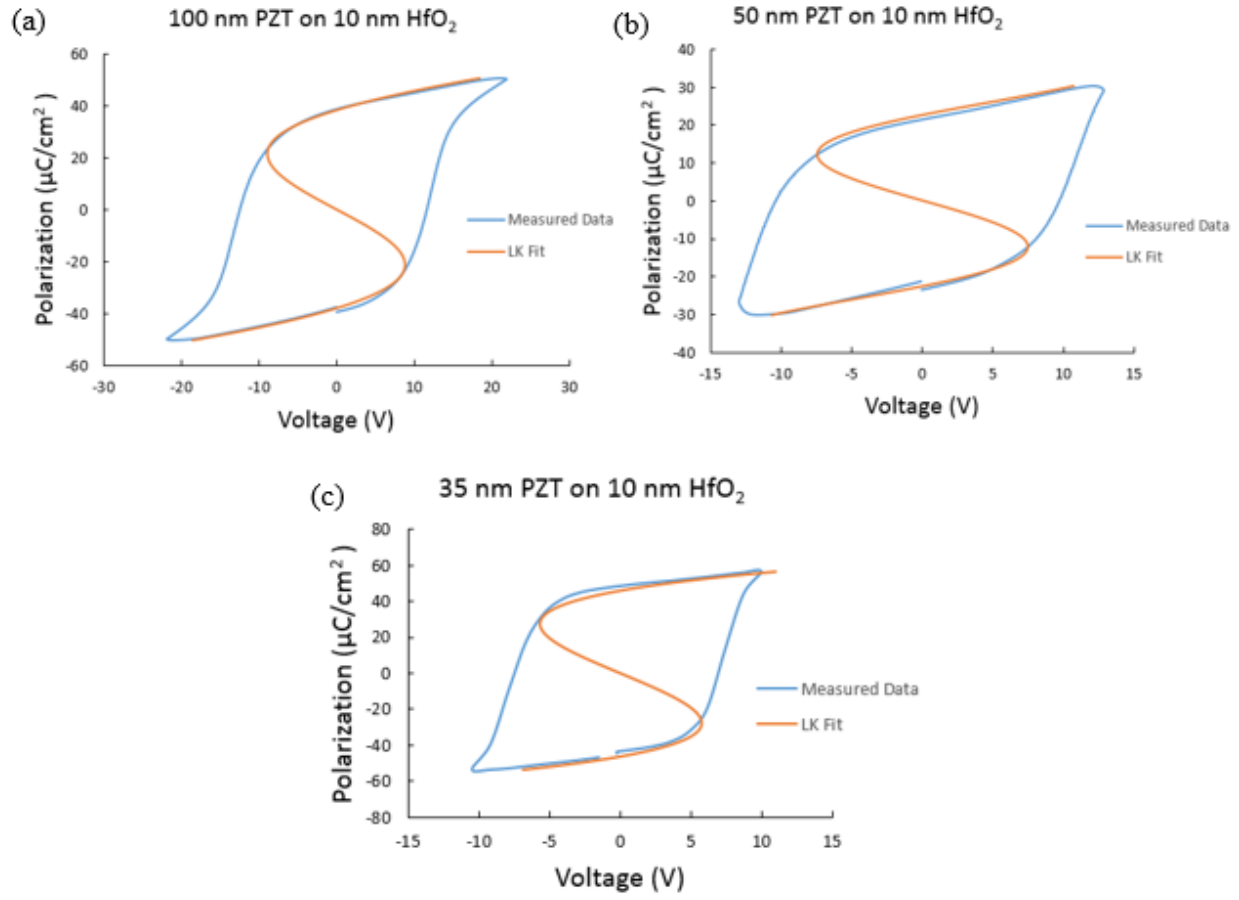

Figure 16 LK curves plotted on the polarization versus voltage hysteresis loops for (a) 100 nm, (b) 50 nm, (c) 35 nm PZT deposited on 10 nm HfO_2. The blue curves represent experimental data and the orange curves are the computationally generated LK fits.

Because capacitance is defined as the charge between two electrodes divided by the voltage between them, the middle of the LK curve where polarization increases as voltage decreases is referred to as an “unstable” region, and represents the region of negative differential capacitance across the ferroelectric.

2. PZT deposited on 100 nm Pt

Figure 17 also shows plots of LK fits for the polarization versus voltage data from ferroelectric capacitors structured with 100 nm and 50 nm of PZT deposited on 100 nm Pt. Because of the work function differences between the heavily doped silicon electrode (~4.05eV) and the nickel electrode (~5.04 eV), the measured polarization versus voltage curves were not centered at the origin. For LK fit calculations, the loops were appropriately shifted laterally to be symmetric about the origin.

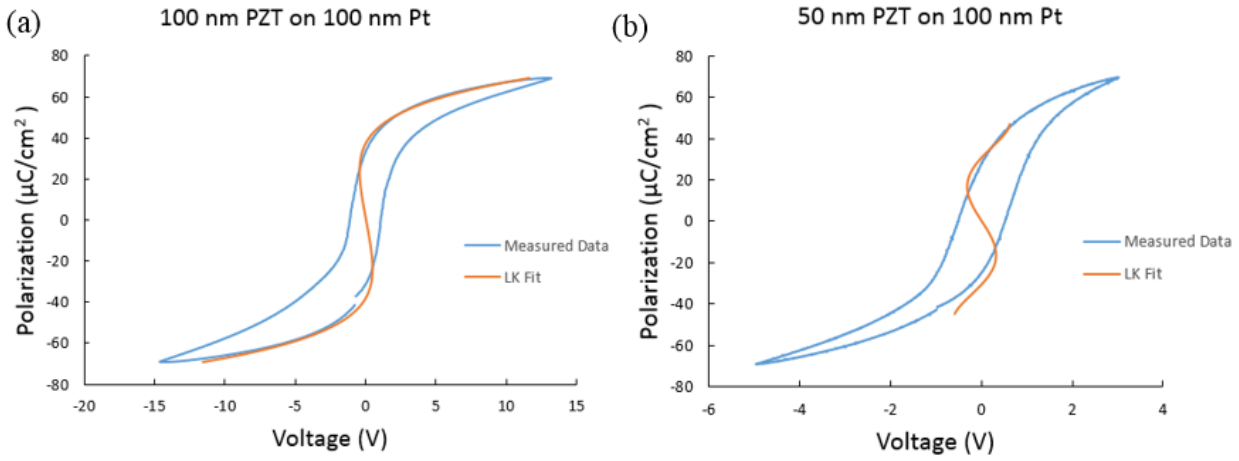

Figure 17 LK fit curves plotted on the polarization versus voltage loops for (a) 100 nm PZT (shifted -0.71 V to be centered about the origin) and (b) 50 nm PZT (shifted -0.98 V) deposited on 100 nm Pt.

3. PZT Deposited on Varying Thicknesses of Pt

The polarization versus voltage data for the ferroelectric capacitor structures with varying Pt thicknesses were more irregularly shaped with inflection points that were not clearly defined. As a result, the LK fit curves for these structures do not precisely fit the experimental data but are still valid approximations. Figure 15 shows the plots of these fits for 100 nm PZT deposited on 100 nm, 50 nm, and 35 nm layers of Pt. The top electrode for the structures in Figure 18 was titanium, and the Pt sat on a 10 nm layer of HfO_2. As in the previous data sets, the loops were shifted laterally to be symmetric about the origin.

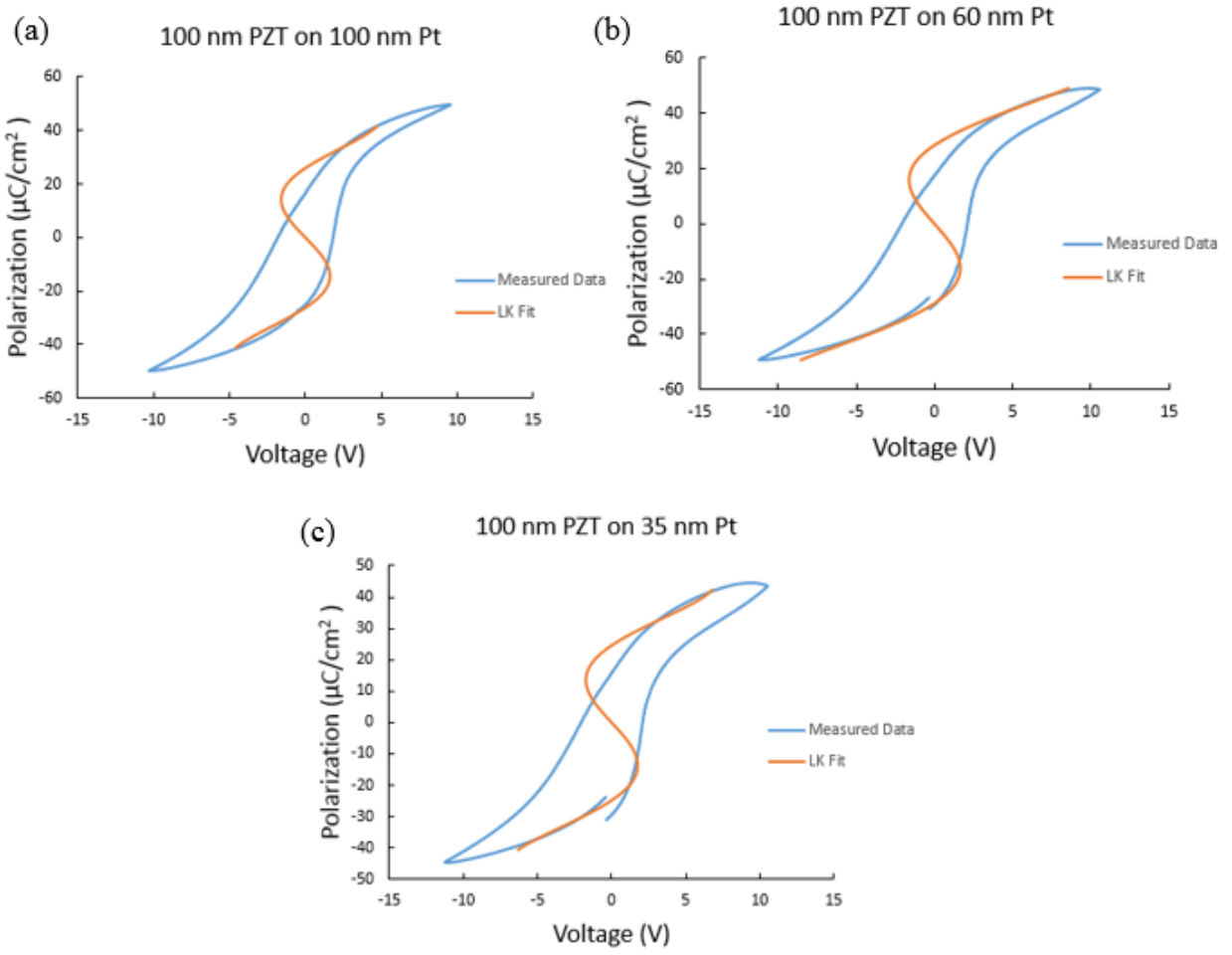

Figure 18 LK fit curves plotted on the polarization versus voltage loops for 100 nm PZT deposited on (a) 100 nm Pt (shifted -0.36 V to be centered about the origin), (b) 60 nm Pt (shifted -0.33 V), (c) 35 nm Pt (shifted -0.38V).

4. Landau Coefficients for all Ferroelectric Capacitor Structures

The Landau Coefficients for the ferroelectric capacitor structures discussed previously are compiled in the following Table 1. These values correspond to the LK fits that were plotted in the previous figures, and were computed using the method involving additional user input to determine the points to fit.

PZT (nm)	Pt (nm)	HfO_2 (nm)	α (m/F)	β ($m^5/F/C^2$)	γ ($m^9/F/C^4$)
100	None	10	-6.3×10^{8}	4.9×10^{9}	-3.9×10^{9}
75	None	10	-1.7×10^{9}	1.3×10^{11}	-1.9×10^{12}
50	None	10	-1.9×10^{9}	4.7×10^{10}	-2.1×10^{11}
35	None	10	-8.7×10^{8}	3.4×10^{9}	3.2×10^{9}
100	100	10	-2.7×10^{7}	9.8×10^{7}	6.5×10^{8}
100	60	10	-1.6×10^{8}	2.2×10^{9}	-3.4×10^{9}
100	35	10	-1.9×10^{8}	3.9×10^{9}	-1.0×10^{10}
50	100	10	-1.9×10^{7}	8.1×10^{7}	-1.9×10^{9}

Table 1 Landau coefficients compiled for various ferroelectric capacitor structures.

These Landau coefficients α, β, and γ are dependent on the shape of the hysteresis loops as well as dielectric constants which are influenced by temperature [11].

Chapter 4: Simulating I-V Characteristics of a FerroFET

To simulate the current – voltage (I-V) characteristics of a ferroFET with given ferroelectric material and thickness, it is possible to first take experimental data describing the electrical behavior of a conventional silicon FET as a baseline. Extracting the charge – voltage relationship for the baseline Si FET is done by first measuring the capacitance – voltage relationship [7]. A voltage is applied to the gate of the FET while the source and drain are grounded and the measured C – V characteristics are integrated to obtain the Q – C relationship. Subsequently, it is necessary to subtract the capacitance contributed from accumulation from the total capacitance so that the resulting Q – V relationship is for the baseline Si FET without the oxide layer having an effect [7].

Then, using the Landau coefficients calculated from the polarization versus voltage data from the ferroelectric capacitor, determine the voltage drop across the ferroelectric layer and sum it in series with the voltage drop across the baseline FET. The “unstable” region of negative capacitance will cause a hysteresis in the I-V curve. The total voltage across both the baseline FET and ferroelectric layer is plotted against the current in forward (increasing) and backward (decreasing) voltage sweeps. Figure 19 is an example of I-V characteristics that were derived from a ferroelectric capacitor and baseline transistor. The calculations assume that the ferroelectric material contribution to the voltage scales linearly with the thickness of the ferroelectric layer. The ferroFET shows a clear gain in current as a result of the negative capacitance region.

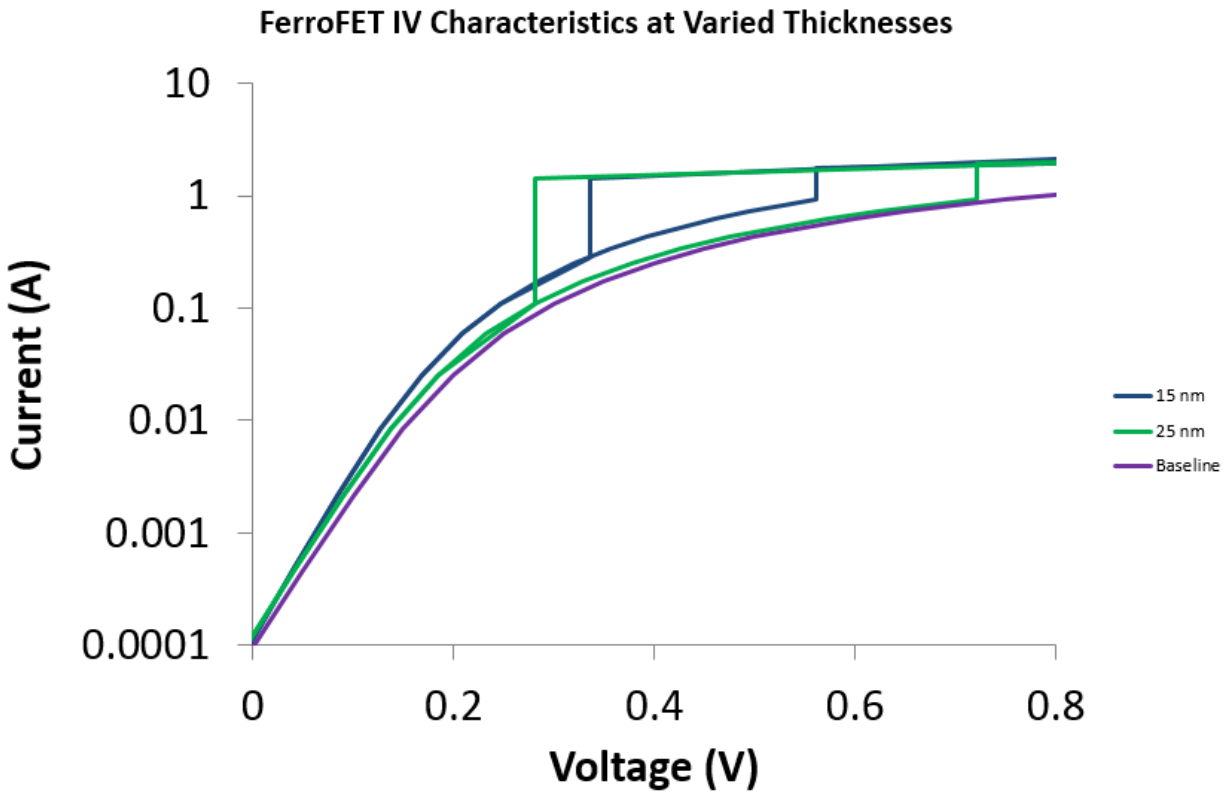

Figure 19 An example of simulated I-V characteristics of a ferroFET with differing thicknesses of the ferroelectric layer compared to the I-V characteristics of the baseline transistor.

The Matlab script to accomplish this first organizes the data points in order of increasing current values and then steps through the voltage values. For the forward voltage sweep, the script checks each voltage value to ensure that voltage increases as current does and plots each point. Any point in which the voltage decreases with an increase in current is removed, and the code continues to step through each voltage value until finding one that is greater than the initial. Then, a linear line is fit between the two points around the removed ones. This process continues until the maximum voltage is reached. The backward voltage sweep process is similar, except that the voltage must decrease with decreasing current, and points that violate this physical principle are removed.

When the result is plotted, as in Figure 19, there is a hysteresis in the I-V curves from the ferroelectric layer. Thicker ferroelectrics show a higher gain, but larger hysteresis over the baseline Si FET.

Chapter 5: Future Work

1. Other Ferroelectric Materials

Ferroelectric field effect transistors have great potential to be the solution to CMOS scaling problems. The low power required switch a ferroFET makes them an energy efficient candidate for the next generation of devices. However, there is still much to be understood about the characteristics and behaviors these transistors. One major goal would be to determine the ideal ferroelectric material for use. This work primarily explores characteristics of the ferroelectric PZT. However, a thin film ferroelectric material with fewer defects and more uniform crystallinity would likely perform closer to the theoretical models based on Landau-Devonshire theory [7]. In addition, the ferroelectric properties of interest are not constant for PZT when thicknesses are scaled down to the 10-30 nm range, and the reduced ferroelectric behavior for thin films would decrease the performance of the devices [7].

Recently, it has been proposed that the antiferroelectric material $HfZrO_2$ (HZO) can be used in FETs for steep switching, low power electronics [12]. Since the oxide is halfnium-based, it is compatible with current CMOS processes while still displaying ferroelectric characteristics. The negative capacitance allows for voltage amplification and a group at the National Taiwan University showed devices able to attain a minimum subthreshold slope of 23 mV/dec and an average subthreshold slope of 50 mV/dec [12]. Thus, HZO may be a suitable material for low power devices.

2. The Quantum Metal FerroFET

An additional issue with some current ferroFET designs is that many ferroelectric materials are not electrically well matched to semiconductors [13]. In order to accomplish steep switching, it is necessary for the negative differential capacitance across the ferroelectric layer summed with the positive capacitance across the other layers to be as close to zero as possible so that small changes in gate voltage will result in large changes in drain current. However, semiconductors do not present a constant capacitive load when going from depletion to inversion [13]. This makes it difficult to ensure low a subthreshold slope for the device. FerroFETs also require homogenous polarization across the device, but this is not always possible due to the mixed domains of the material [13].

One solution is a proposed quantum metal ferroFET, which involves depositing a very thin layer of metal between the semiconductor and ferroelectric layer [13]. The metal layer is so thin that it behaves as a 2D electron gas and presents a constant "quantum capacitance" to the ferroelectric layer [13]. Because the layer is extremely thin, it has a low charge carrier density and therefore can have a changing work function as the polarization of the ferroelectric layer changes, attenuating large charge swings within the ferroelectric [13]. The quantum metal ferroFET has not yet been fabricated, and so the next step would be to create the device and compare its performance to the predictions.

Overall, ferroFETs show great promise in the field of low power electronics as CMOS devices reach their scaling limits. Future work on this topic will need to determine the ideal ferroelectric material, address ferroelectric-semiconductor mismatch issues, and obtain a greater understanding of the ferroFET device behaviors.

Appendix A: Matlab Code for LK Fit (P-E Data Input Only)

```
%read in data
dataPoints = 'insert file path here';
P = xlsread(dataPoints, 'B:B');
V = xlsread(dataPoints, 'A:A');

%Vmin, Vmax, and indices
[Vmin, Imin] = min(V);
[Vmax, Imax] = max(V);

%points for linear fit
Vlin(1) = V(Imin);
Vlin(2) = V(Imax);
Vlin(3) = 0;
Plin(1) = P(Imin);
Plin(2) = P(Imax);
Plin(3) = 0;

flin = polyfit(Vlin,Plin,1);

%generate curves 1 and 2
C1index = 1;
C2index = 1;
for i=1:length(V)
    if P(i) > polyval(flin,V(i))
        C1V(C1index) = V(i);
        C1P(C1index) = P(i);
        C1index = C1index+1;
    end
    if P(i) < polyval(flin,V(i))
        C2V(C2index) = V(i);
        C2P(C2index) = P(i);
        C2index = C2index+1;
    end
end

%fit polynomials to curves 1 and 2
fC1 = polyfit(C1V,C1P,10);
fC2 = polyfit(C2V,C2P,10);

%get the parts of the data to fit LK
firstDer1 = polyder(fC1);
secondDer1 = polyder(firstDer1);
```

```
thirdDer1 = polyder(secondDer1);

%Curve 1 derivative tests: first=+, second=-, third=0
r = roots(thirdDer1);
for i=1:length(r)
    try
        if r(i)>max(C1V) || r(i)<min(C1V)
            r(i)=[];
        end
    catch exception
        %if elements are deleted, length(r) will go out of
bounds
    end
end

for i=1:length(r)
    if polyval(secondDer1,r(i))<0
        if polyval(firstDer1,r(i))>0
            if exist('cutoffV1', 'var') == 1
                if
polyval(firstDer1,r(i))>polyval(firstDer1,r(cutoffIndex))
                    cutoffV1 = r(i);
                    cutoffIndex = i;
                end
            end
            if exist('cutoffV1', 'var') == 0
                cutoffV1 = r(i);
                cutoffIndex = i;
            end
        end
    end
end

%Curve 2 derivative tests: first=+, second=+, third=0
firstDer2 = polyder(fC2);
secondDer2 = polyder(firstDer2);
thirdDer2 = polyder(secondDer2);

r2 = roots(thirdDer2);
for i=1:length(r2)
    try
        if r2(i)>max(C2V) || r2(i)<min(C2V) || r2(i)<0
            r2(i)=[];
        end
    catch exception
```

```
        %if elements are deleted, length(r2) will go out of
bounds
    end
end

for i=1:length(r2)
    if polyval(secondDer2,r2(i))>0
        if polyval(firstDer2,r2(i))>0
            if exist('cutoffV2','var') == 1
                if abs(polyval(firstDer2,r2(i))-flin(1)) <
abs(polyval(firstDer2,r2(cutoffIndex))-flin(1))
                    cutoffV2 = r2(i);
                    cutoffIndex = i;
                end
            end
            if exist('cutoffV2','var') == 0
                cutoffV2 = r2(i);
                cutoffIndex = i;
            end
        end
    end
end

%only keep points close to LK curve
LKindex = 1;
for i=1:length(C1V)
    if C1V(i)>=(cutoffV1-max(V)*0.1)
        LK1V(LKindex) = C1V(i);
        LK1P(LKindex) = C1P(i);
        LKindex = LKindex+1;
    end
end


LKindex = 1;
for i=1:length(C2V)
    if C2V(i)<=(cutoffV2+max(V)*0.1)
        LK2V(LKindex) = C2V(i);
        LK2P(LKindex) = C2P(i);
        LKindex = LKindex+1;
    end
end


LKV = [LK1V LK2V];
LKP = [LK1P LK2P];
```

```
A = [LKP; LKP.^3; LKP.^5];
syms a b c;
X = [a b c];

ERR = LKV - X*A;

S = ERR.^2;
sqSum = sum(S);
EQ1 = diff(sqSum,a);
EQ2 = diff(sqSum,b);
EQ3 = diff(sqSum,c);
[alpha,beta,gamma]=solve(EQ1,EQ2,EQ3);
double(alpha)
double(beta)
double(gamma)


%calculate V values for P = [min,max] from LK fit
Ptest = linspace(min(P),max(P),200);
for i=1:length(Ptest)
    Vtest(i) = alpha*Ptest(i) + beta*(Ptest(i))^3 +
gamma*(Ptest(i))^5;
end

plot(V,P,'o')
hold on
plot(Vtest,Ptest,'g')
title('Method 1')
xlabel('E (MV/cm)')
ylabel('P (uC/cm2)')

V1 = linspace(-10,10,100);
P1 = polyval(flin,V1);
figure
plot(V1,P1)
hold on
plot(C1V,C1P,'gd')
plot(C2V,C2P,'ro')
plot(C1V,polyval(fC1,C1V),'bx');
plot(C2V,polyval(fC2,C2V),'c*');
figure
plot(LK1V,LK1P,'rd')
hold on
plot(LK2V,LK2P,'rd')
```

Appendix B: Matlab Code for LK Fit (P-E Data and Additional User Input)

```
%read in data
dataPoints = 'insert file path here';
P = xlsread(dataPoints, 'B:B');
V = xlsread(dataPoints, 'A:A');

%plot input data and prompt for user specified points
plot(V,P,'o')
[LKV,LKP] = ginput;
title('Method 2')
xlabel('E (V/cm)')
ylabel('P (C/cm2)')

LKV = LKV.';
LKP = LKP.';

A = [LKP; LKP.^3; LKP.^5];
syms a b c;
X = [a b c];

ERR = LKV - X*A;

%sum of least squares error
S = ERR.^2;
sqSum = sum(S);
EQ1 = diff(sqSum,a);
EQ2 = diff(sqSum,b);
EQ3 = diff(sqSum,c);
[alpha,beta,gamma]=solve(EQ1,EQ2,EQ3);
double(alpha)
double(beta)
double(gamma)

%generate the LK fit
Ptest = linspace(min(P),max(P),200);
for i=1:length(Ptest)
    Vtest(i) = alpha*Ptest(i) + beta*(Ptest(i))^3 +
gamma*(Ptest(i))^5;
end

hold on
plot(Vtest,Ptest,'g')
```

Appendix C: Matlab Code for I-V Simulations

```
dataPoints = 'insert file path here';
I = xlsread(dataPoints, 'A:A');
V = xlsread(dataPoints, 'B:B');

semilogy(V,I,'bx', 'MarkerSize',15)
xlabel('Total Voltage (V)')
ylabel('Current (A/um)')
points = [I V];

%order by increasing I
points = sortrows(points);
p2index = 1;
j=1;

%forward V sweep
while j<length(points)
    V1 = points(j,2);
    V2 = points(j+1,2);
    I1 = points(j,1);
    I2 = points(j+1,1);

    if V2<V1
        foundNextpt = 0;
        counter = 1;
        while foundNextpt==0
            if points(j+counter,2)>V1
                V3 = points(j+counter,2);
                I3 = points(j+counter,1);

                V4 = points(j+counter-1,2);
                I4 = points(j+counter-1,1);
                foundNextpt = 1;
            end
            counter = counter + 1;
        end

        x(1)=V3;
        x(2)=V4;
        y(1)=I3;
        y(2)=I4;
```

```
        flin = polyfit(x,y,1);

        Itemp = polyval(flin,V1);

        pointsfor(p2index,1) = Itemp;
        pointsfor(p2index,2) = V1;
        p2index = p2index+1;

        j = j + counter;

    else
        if p2index ==1
            pointsfor(p2index,1) = I1;
            pointsfor(p2index,2) = V1;
            pointsfor(p2index+1,1) = I2;
            pointsfor(p2index+1,2) = V2;
            p2index = p2index+2;
            j=j+1;
        else
            pointsfor(p2index,1) = I2;
            pointsfor(p2index,2) = V2;
            p2index = p2index+1;
            j=j+1;
        end
    end
end
hold on
semilogy(pointsfor(:,2),pointsfor(:,1),'g','LineWidth',4)

%backwards V sweep
k=length(points);
pbindex = 1;
while k>1
    V1 = points(k,2);
    V2 = points(k-1,2);
    I1 = points(k,1);
    I2 = points(k-1,1);

    if V2>V1
        counter = 2;
        ktemp = k;
        while ktemp>1
            try
                V3 = points(k-counter,2);
                V4 = points(k-counter-1,2);
                I3 = points(k-counter,1);
```

```
                I4 = points(k-counter-1,1);
            catch
                ktemp=0;
                k=0;
            end

            if V3<V1
                x(1)=V3;
                x(2)=V4;
                y(1)=I3;
                y(2)=I4;
                flin = polyfit(x,y,1);

                Itemp = polyval(flin,V1);
                pointsback(pbindex,1) = Itemp;
                pointsback(pbindex,2) = V1;
                pbindex = pbindex+1;
                ktemp=0;
                k=k-counter;
            end
            ktemp=ktemp-1;

            counter = counter+1;
        end

    else
        if k==length(points)
            pointsback(pbindex,1)=I1;
            pointsback(pbindex,2)=V1;
            pointsback(pbindex+1,1)=I2;
            pointsback(pbindex+1,2)=V2;
            pbindex = pbindex+2;
        else
            pointsback(pbindex,1)=I2;
            pointsback(pbindex,2)=V2;
            pbindex = pbindex + 1;
        end
    end
    k = k - 1;
end
semilogy(pointsback(:,2),pointsback(:,1),'r--','LineWidth',4)
legend('Measured data', 'Forward sweep', 'Backwards sweep')
```

Bibliography

[1] W. Haensch, E. J. Nowak, R. H. Dennard and e. al., "Silicon CMOS devices beyond scaling," *IBM Journal of Research and Development,* vol. 50, no. 4.5, pp. 339-361, 2006.

[2] T. N. Theis and P. M. Solomon, "In quest of the next switch: Prospects for greatly reduced power dissipation in a successor to the silicon field-effect transistor," *Proceedings of the IEEE,* vol. 98, no. 12, pp. 2005-2014, 2010.

[3] S. Salahuddin and S. Datta, "Use of negative capacitance to provide voltage amplification for low power nanoscale devices," *Nano Letters,* vol. 8, no. 2, pp. 405-410, 2008.

[4] G. Catalan, D. Jiménez and A. Gruverman, "Ferroelectrics: Negative capacitance detected," *Nature Materials,* vol. 14, no. 2, pp. 137-139, 2015.

[5] A. I. Khan, K. Chatterjee, B. Wang, S. Drapcho and e. al., "Negative capacitance in a ferroelectric capacitor," *Nature materials,* vol. 14, no. 2, pp. 182-6, 2015.

[6] P. Chandra and P. Littlewood, A Landau Primer for Ferroelectrics, 2008.

[7] S. Dasgupta, A. Rajashekhar, K. Majumdar and e. al., "Sub-kT/q Switching in Strong Inversion in PbZr0.52Ti0.48O3 Gated Negative Capacitance FETs," *IEEE Journal on Exploratory Solid-State Computational Devices and Circuits,* vol. 1, pp. 43-48, 2015.

[8] C. L. Wang and S. R. Smith, "Landau theory of the size-driven phase transition in ferroelectrics," *Journal of Physics: Condensed Matter*, vol. 7, no. 36, pp. 7163-7171, 1995.

[9] M. Stewart and M. G. Cain, "Ferroelectric Hysteresis Measurement & Analysis," National Physical Laboratory, University of Manchester, 1999.

[10] J. T. Evans, "Operating the Radiant TO-18 Sawyer-Tower Board," Radiant Technologies, Inc., 2016.

[11] T. K. Song, "Landau-Khalatnikov Simulations for Ferroelectric Switching in Ferroelectric Random Access Memory Application," *Journal of the Korean Physical Society*, vol. 46, no. 1, pp. 5-9, 2005.

[12] M. H. Lee, Y. -T. Wei, K.-Y. Chu, J.-J. Huang and C.-W. Chen, "Steep Slope and Near Non-Hysteresis of FETs With Antiferroelectric-Like HfZrO for Low-Power Electronics," *IEEE Electron Device Letters*, vol. 36, no. 4, pp. 294-296, 2015.

[13] D. Frank, P. Solomon, C. Dubourdieu and M. Frank, "The Quantum Metal Ferroelectric Field-Effect Transistor," *IEEE Transactions on Electron Devices*, vol. 61, no. 6, pp. 2145-2153, 2014.

ACADEMIC VITA

VICTORIA L. CHEN

EDUCATION

Bachelor of Science in Engineering Science **May 2016**

- The Pennsylvania State University (University Park, PA)
- Schreyer Honors College Scholar
- Nanotechnology focus
- Minors in Physics and Economics
- Member of Tau Beta Pi

RESEARCH EXPERIENCE

Undergraduate Research Assistant – Nanoelectronic Devices and Circuits Lab, Penn State
Research Advisor: Professor Suman Datta *August 2014–present*

- Computationally simulate current and voltage characteristics of ferroelectric field effect transistors (ferroFETs), calculating for different thicknesses of the ferroelectric material layer
- Write MatLab code to fit Landau-Khalatnikov (LK) curves to polarization-voltage data of ferroelectric materials

PROFESSIONAL EXPERIENCE

Geometry Tutor – Volunteers in Public Schools (State College, PA) *November 2014–present*

- Tutor high school students in advanced and college preparatory geometry concepts

Technology Development Intern – Intel Corporation (Aloha, OR) *May–August 2015*

- Developed and evaluated new wafer probing technologies for Silicon Bridge project
- Characterized wafer probe materials
- Performed statistical data analysis with JMP and JSL
- Presented results and data to upper management

Technology Development Intern – Intel Corporation (Hillsboro, OR) *January–August 2014*

- Audited electrical components on Printed Circuit Board of Sort Interface Unit
- Developed qualification process for approving electrical component use
- Worked on system for isolating and preventing wafer probe failure
- Assisted in drafting patent for probe failure isolation technology

PUBLICATIONS

A. Letourneur, **V. Chen**, G. Waterman and P. J. Drew, "A method for longitudinal, transcranial imaging of blood flow and remodeling of the cerebral vasculature in postnatal mice," Physiological Reports, vol. 2, no. 12, pp. 1-10, 2014.

AWARDS

- Stanford Graduate Fellowship *February 2016*
- Mirna Urquidi-Macdonald and Digby D. Macdonald Student Award in ESM *August 2013*
- Summer Discovery Research Grant *May 2013*
- Penn State President's Freshman Award *April 2012*
- NASA Pennsylvania Space Grant *December 2011*